Final Report, OTKA NN 107776

(Miklós Nyitrai)

HUMAN RESOURCES

The team has been changed since the beginning of the project. Zoltán Ujfalusi went for a two-year fellowship in Canterbury, England in February, 2014. Katalin Türmer became a mom and was on maternity leave between May, 2014 and October 2015. In the meantime, Szilvia Barkó came back from maternity leave and joined the team in September, 2014. Emőke Bódis came back in September 2014 from a one-year study trip in Gainesville (UF, USA), where she did research in Michael Bubb's laboratory. Dávid Szatmári spent two years in the laboratory of our collaboration partner, Robert C. Robinson, and came back to joined our team in September, 2014. Although these changes put challenges on the project, we completed all the scientific aims by the end of the project period.

TECHNICAL PROBLEMS DURING THE PROJECT

After we did the preliminary experiments described in our previous report, we discovered that the preparation of the MreB from *Leptospira interrogans* results in more than one major protein populations. Detailed analyses of the observations showed that one of the two populations contained some lipid contamination, and was probably in an altered conformation compared to the main population. This contamination proved to be very difficult to remove. We consult this problem with other international labs, including our collaboration partner as well, and no clear solution was provided. Systematically testing the possible solutions we found out in November, 2014 that denaturation of the preparation in its middle stage can help to solve this problem. Under special conditions we managed to remove the contaminations and now can produce the MreB in sufficient quantities and appropriate purity as well. This new preparation allowed us to repeat all of the previous experiments, and we found that the initial observations were correct. We used several fluorescent phalloidin derivatives to test whether phalloidin can bind to MreB. All these tests confirmed the phalloidin binding, and shed light on the conditions where the binding is more pronounced. We also express now MreB from other bacterial sources (e.g. *Thermotoga maritime* and *E.coli*) so these could provide the proper and previously characterised reference protein systems for our investigations.

These problems resulted in the delay of the experimental plan. By the end of 2015 we completed almost all the planned MreB experiments successfully, but the publications of these results are still in progress. We have submitted a manuscript in the beginning of December, 2015 describing the details of the new protein purification protocol and also the polymerisation properties we characterised by labelling the MreB with fluorophores. This manuscript is under review and also attached to this final report. We also have a manuscript under preparation that will describe the interactions between MreB and phalloidine, and a third one that will provide a comprehensive characterisation regarding the salt and ionic strength dependence of the assembly of MreB. The former will be submitted in appr. a month, the latter by May.

SUMMARY OF THE RESULTS ACHIEVED IN THE PROJECT

The aim of the project was to describe and understand the structural and functional properties of bacterial protein filaments. The investigations were carried out in collaboration with Robert C. Robinson's laboratory from Singapore. In the first part of the project we developed and improved the method of purification of MreB from *Leptospira interrogans*. Now one preparation yields 5-10 mg protein, which is enough for biophysical studies and will also properly serve the aims of structural investigations. Parallel to these investigations I visited the Singaporean lab to discuss the first set of results and finalize the plans for the future research.

We study the conformational and dynamic properties of MreB by using spectroscopic methods. We attempted to label the protein for these studies with a fluorophore and / or spin probe. We observed, that only one of the two cysteines was labelled under the given conditions, which renders this labelling suitable for our investigations. To find out which of the two amino acids is attached to the probe, we will carried out mass spectroscopy experiments. In the mean time we established that the labelling of the MreB did not influence the polymerization properties of the protein. We investigated both the monomeric and filamentous forms of the MreB by applying the novel spectroscopic probes and various biophysical methods. The first set of data indicated that the protein matrix around the label is much more flexible than in actin.

In agreement with the experimental plans we also investigated the exciting interaction between MreB and fluorescent phalloidine. We confirmed the binding by using fluorescence microscopic and steady-state spectroscopic methods. So far, no other MreB isoform was shown to bind this toxic peptide. Therefore, our first aim is to describe the binding, the affinity, and the results of binding in terms of conformational changes. For these we applied various biochemical methods and spectroscopic techniques as well. Once these data were established, we carried out structural and functional studies under *in vitro* conditions and also in bacterial cells. To foster this approach we visited this May Alf Mansson in Kalmar and learnt how to measure the persistence length of the filaments by applying microscopic and mathematical methods.

We also extended our studies for the investigations of MreB localization in bacterial cells. As these bacteria are disease causing pathological cells, we paid special attention when handling them. For this purpose we collaborate with the Microbiology Department of the University of Pécs. So far we obtained the required *Leptospira* interrogans cell lines and now we move on to modify and characterize them.

By the second part of the project we started the preliminary works on the structural aspects too. Currently we aim to produce large quantities of MreB for these works. Once we have enough protein we will send it to Singapore, and the electron microscopy and X-ray chrystallography investigations will be started. In the case of X-ray studies it is more difficult to predict when the data will become available due to the uncertainty attributed to the crystallization procedures.

Apart from the investigations with MreB we also carried out several studies in eukaryotic cytoplasmic proteins. The results of these investigations will serve as references for our

prokaryotic works, and also facilitate the further development of the biophysical and other experimental tools we plan to use for the MreB studies.

The results we obtained with MreB isoforms were presented in the following national and international conferences:

1. EMBO Workshop on a Systems-Level View of Cytoskeletal Function
   October 27-31, 2014, Stockholm, Sweden.
2. 45. Membrán-Transzport Konferencia
   May 19-22, 2015, Sümeg, Hungary.
3. Polymers and Self- Assembly: From Biology to Nanomaterials
   October 25-30, 2015, Rio de Janeiro, Brazil.

During the project we published 10 papers based on the results. All these papers are listed in the appropriate page of the OTKA web site. The weakness of this report is that the results we obtained focusing directly on the properties and functions of MreB are still to be published, due to the difficulties we experienced during the project. The manuscript of the paper we just submitted is attached to the end of this report.

The manuscript submitted (6th of December, 2015) based on the results of the project:

Large-scale purification and *in vitro* characterisation of the assembly of MreB from *Leptospira interrogans*

Szilvia Barkó[*a], Dávid Szatmári[*a], Emőke Bódis[a], Katalin Türmer[a], Zoltán Ujfalusi[a], David Popp[b], Robert C. Robinson[b,c] and Miklós Nyitrai[a, d, e]

[a] Department of Biophysics, Medical School, University of Pécs, Szigeti str. 12, Pécs, H-7624, Hungary

[b] Institute of Molecular and Cell Biology, A*STAR (Agency for Science, Technology and Research), Biopolis, Singapore 138673

[c] Department of Biochemistry, Yong Loo Lin School of Medicine, National University of Singapore, Singapore 117597

[d] MTA-PTE Nuclear-Mitochondrial Interactions Research Group, Szigeti str. 12, Pécs, H-7624, Hungary

Keywords: MreB, bacterial actin, cytoskeleton, polymerization, fluorescence microscopy.

[e] corresponding author

[*] equal contributions

ABSTRACT

BACKGROUND

Wiel's syndrome is caused by *Leptospira interrogans* infections, a Gram negative bacterium with a distinct thin corkscrew cell shape. The molecular basis for this unusual morphology is unknown. In many bacteria cell wall synthesis is orchestrated by the actin homolog, MreB.

METHODS

Here we have identified the MreB within the *Leptospira interrogans* genome and expressed the His-tagged protein product of the synthesized gene (*Li*-MreB) in *E. coli*. *Li*-MreB did not purify under standard nucleotide-free conditions used for MreBs from other species, requiring the continual presence of ATP to remain soluble. Covalent modification of *Li*-MreB free thiols with Alexa488 produced a fluorescent version of *Li*-MreB.

RESULTS

We developed native and denaturing/refolding purification schemes for *Li*-MreB. The purified product was shown to assemble and disassemble in $MgCl_2$ and KCl dependant manners, as monitored by light scattering and sedimentation studies. The fluorescent spectrum of labelled *Li*-MreB-Alexa488 showed cation-induced changes in line with an activation process followed by a polymerization phase. The resulting filaments appeared as bundles and sheets under the fluorescent microscope. Finally, since the *Li*-MreB polymerization was cation dependant, we developed a simple method to measure monovalent cation concentrations within a test case prokaryote, *E. coli*.

CONCLUSIONS

We have identified and initially characterized the cation-dependent polymerization properties of a novel MreB from a non-rod shaped bacterium and developed a method to measure cation concentrations within prokaryotes.

GENERAL SIGNIFICANCE

These initial characterizations of *Li*-MreB will enable future structural determination of the MreB filament from this corkscrew shaped bacterium.

INTRODUCTION

A functioning cell wall is crucial for the reproduction and survival of bacteria (1). It defines cell shape and acts as a barrier to separate internal and external conditions, protecting against challenges such as osmotic pressure differences (2, 3). Within most rod-shaped bacteria, the constituents of the cell wall peptidoglycan layer are synthesized by an intracellular enzyme machinery. The actin ortholog MreB has an indispensable role in coordinating peptidoglycan synthesis and the insertion of the newly synthesized patterns into the cell wall (4). As such, MreB is an essential protein in orchestrating the spatial and temporal cell morphologies of many bacteria. Exposing cells to an MreB polymerisation-inhibitor (A22) causes the loss of their characteristic rod shape (5), leads to deviant localization of several membrane proteins (6) and results in a decrease in cell rigidity (7). Comparison of crystal structures of proteins that are comprised of the 'actin fold' reveals structural homology despite the poor sequence homology between MreB (*Thermotoga maritima*) (8), the plasmid segregating protein ParM-R1 (*E. coli*) (9–11), and eukaryotic actin. This structural similarity between the monomers of MreB and actin translates into similarities in polymerization, in that MreB also forms long filaments (12) and other structures (13). However, the variety of MreB structures and the range of MreB functions have not been characterized across the range of cell shapes adopted by diverse bacterial species.

Characterization of the *in vitro* polymerisation of MreB has produced conflicting results. Similar to actin, MreB polymerisation requires Mg^{2+} and ATP. The critical concentration for polymerisation of MreBs from different species have been reported to range between 3 nM and 1.5 μM (14, 15). MreB polymerisation is sensitive to the concentrations of monovalent cations with the rate of the polymerization declining with increasing KCl concentrations (15). It has yet to be elucidated why the physiological K^+ concentrations found in bacteria (300-500 mM) inhibit the extent of polymerisation. One explanation can be that high KCl concentrations may prevent MreB from spontaneous assembly while allowing for site-specific assembly. MreB polymerization is also sensitive to the type of bound nucleotide. The highest polymerisation rate is achieved with ATP (similar to GTP) while the polymerisation is almost inhibited in the presence of UTP and CTP (15). For *Thermotoga maritima* MreB (*Tm*-MreB), polymerisation can be initiated with the addition of ATP and the rate of polymerisation is significantly quicker than that of actin. The rate of polymerization increases with $MgCl_2$ concentration (14), while varying $CaCl_2$ concentration does not have a marked influence.

Early reports of the *in vivo* structures of MreB assemblies in living cells (*B. subtilis*) using fluorescein-labelled vancomycin indicated that the MreB filamentous system associates with the inner membrane of the cell, forming a large helix between the poles of the bacteria (16). These observations were based on total internal reflection fluorescence microscopy. More recent super-resolution and total internal reflection fluorescence microscopic techniques support a model that MreB forms shorter helical pieces, seen as patches, that associate to the inner membrane throughout the cell and localize to the cell-wall synthesis machineries (17, 18).

The phylum *Spirochetes* comprises organisms that have distinct cellular morphologies that range from helical to flat wave-shaped cells. *Leptospira interrogans* has a long (~10 μm) but thin (~0.2 μm) helical cell shape and its motility is driven by the rotation of two periplasmic flagella. Using the flagella and a corkscrew motility, *Leptospirae* gain an advantage in spreading during infection. Leptospirosis is an emerging global zoonotic disease. Acute manifestations of leptospirosis, in the forms of severe pulmonary haemorrhage syndrome and Weil's disease, have significant mortality rates, > 50 % and > 10 %, respectively (22). Since the characteristic helical morphology of the cell is remarkably different from rod-shaped bacteria, it is interesting to understand the molecular basis of the formation and maintenance of the helical shape. Currently it is not known whether these cells rely on a different orchestration of their peptidoglycan synthesizing enzymatic machinery, nor which proteins participate in the process. Despite this, the MreB from *Leptospira interrogans* (*Li*-MreB) is likely to have a role in controlling cell morphology (23). Here we have characterised the *in vitro* properties of *Li*-MreB and we compare these activities to those of MreBs from other species. Variations in MreB properties derived from divergent species will help to understand the construction of the diversity in morphologies displayed by bacteria.

MATERIALS AND METHODS

Protein expression, purification and labelling

The *Leptospira interrogans* MreB gene (gene bank accession number: 1152102) was identified by sequence similarity searches to *E. coli* MreB, and the sequence was codon optimized for expression in *Escherichia coli*, synthesized (GenScript) and engineered into the pSY5 plasmid (Novagen), which encodes an 8-histidine tag, followed by a PreScission protease (GE Healthcare Life Sciences) cleavage site prior to the protein sequence (NP_712940). The construct was verified by DNA sequencing. The DNA construct encoding MreB was transformed into the *Escherichia coli* BL21 DE3 pLysS strain (Novagen). Cell cultures were grown in Luria Broth (LB) media at 37 ^{o}C supplemented by ampicillin until reaching OD_{600} = 0.6. Protein expression was induced by adding IPTG to a final concentration of 0.5 mM at 25 ^{o}C overnight. Cells were harvested by centrifugation and pellets were stored at - 20 ^{o}C.

We applied two methods for protein expression. Firstly, a frozen cell pellet (2-3 g) was resuspended in lysis buffer (5 mM imidazole, 2 mM ATP, 2 mM $MgCl_2$, 100 mM KCl, pH 7.5) homogenized and sonicated. After subsequent freezing-thawing cycles (three times), the cell extract was clarified by centrifugation (15,000 x g at 4 ^{o}C for 20 min). The supernatant was loaded onto a Ni-nitrilotriacetic acid (Ni-NTA) (Qiagen) column, which was pre-equilibrated in lysis buffer and was incubated overnight at 4 ^{o}C. The column was washed with three bed volumes of lysis buffer then with increasing concentrations of imidazole (10-350 mM) in lysis buffer. The *Li*-MreB containing fractions were collected and dialysed overnight against buffer A (4 mM TRIS-HCl, 0.1 mM $CaCl_2$, 0.2 mM ATP, 0.5 mM DTT, pH 8.0). The samples were clarified by ultracentrifugation (100,000 x g at 4 ^{o}C for 30 min), and either used immediately, or flash-frozen at liquid nitrogen temperature in small aliquots. The purity of *Li*-MreB was analysed by SDS-PAGE.

In the second strategy, a denaturant was applied during the purification. A frozen cell pellet (2-3 g) was resuspended and homogenized in a denaturing lysis buffer containing 6 M guanidine-HCl, 0.1 M NaH_2PO_4, 10 mM TRIS-HCl, pH 8.0. After centrifugation (30,000 x g at 4 ^{o}C for 30 min) the supernatant was loaded onto a denaturing lysis buffer-equilibrated Ni-NTA column and incubated overnight at 4 ^{o}C. The column was then washed with a buffer containing 8 M urea, 0.1 M NaH_2PO_4, 10 mM TRIS-HCl and a descending pH gradient from pH 8.0 to 4.0 was applied to elute the protein. *Li*-MreB containing fractions were pooled and

applied to a Sephadex G25 column that had been equilibrated with buffer A, in order to refold the *Li*-MreB. The eluted fractions containing *Li*-MreB were pooled and subjected to ultracentrifugation (100,000 x g, 4 ^{o}C, 30 min). The renatured *Li*-MreB was either used immediately or flash-frozen in small aliquots at liquid nitrogen temperature. Concentrations of *Li*-MreB from both purifications were determined by the BCA Protein Assay (Bio-Rad).

The cysteines of *Li*-MreB were labelled with Alexa Fluor® 488 C5 Maleimide. Prior to initiating the labelling reaction DTT was removed using a PD10 (GE Healthcare) buffer exchange column. The concentration of protein was determined using the BCA Protein Assay (Bio-Rad), and the *Li*-MreB solution was incubated in the presence of 5-fold molar excess of Alexa Fluor® 488 C5 Maleimide (overnight on ice). The excess fluorophore was removed by applying the mixture to a Sephadex G25 column equilibrated with buffer A supplemented with 10 mM DTT. The labelled *Li*-MreB was subjected to ultracentrifugation (100,000 x g, at 4 ^{o}C for 30 min), the concentrations of the *Li*-MreB and the fluorophore in the supernatant were determined using the BCA Protein Assay (Bio-Rad) and spectrophotometry, respectively. The ratio of labelling was calculated as the ratio of the label to the protein concentration and was found to be 50 %.

Polymerisation assays

The polymerisation kinetics of *Li*-MreB was investigated using light scattering assays with a Perkin Elmer LS-50 spectrofluorimeter or a Horiba Jobin Yvon fluorimeter. Excitation and emission monochromators were set to 400 nm and the excitation and emission slits to 2.5 mm. The samples (2 ml) were stirred with a magnetic stirrer during the polymerisation process. Polymerisation was initiated by adding monovalent or divalent cations. When Alexa488-labelled *Li*-MreB was used the polymerisation was monitored by changes in the fluorescence intensity signal. The excitation and emission wavelengths were set to 493 nm and 535 nm with a 2 nm slit pair. Rapid fluorescence signal changes were measured using a stopped flow apparatus (SX.18MV-R Stopped Flow Reaction Analyzer, Applied Photophysics).

For the depolymerisation assays, 50 μM Alexa 488 labelled *Li*-MreB was first polymerised for 4 h at room temperature. The depolymerisation of *Li*-MreB was induced by dilution in buffer A or in buffer A supplemented with 2 mM $MgCl_2$ and 100 mM KCl and the fluorescence signal was monitored over time.

Polymerisation equilibria were followed by using SDS-PAGE. To characterise the effect of nucleotides *Li*-MreB was incubated overnight at 20 ^{o}C under different KCl, $MgCl_2$ and nucleotide (ATP, ADP) concentrations. The samples were subjected to ultracentrifugation (100,000 x g at 4 ^{o}C for 30 min) and the pellets and supernatants were analysed with SDS-PAGE.

Fluorescence microscopy

The gross morphologies of the *Li*-MreB-Alexa488 assemblies were investigated using an Olympus IX 81 inverted microscope. In these experiments 20 mM of *Li*-MreB-Alexa488 was incubated in presence of various buffer conditions (buffer A, or 4 mM $CaCl_2$, or 2 mM $MgCl_2$ and 100 mM KCl). 5 µL of each sample was dropped on a slide, covered by a coverslip, and visualised with microscope using a 100 x objective lens (NA 1.4) and a CCD camera (Orca ERG Hamamatsu).

Determination of intracellular salt concentration of E. coli cells

To measure the salt concentration in bacteria, 200 µL of an *E. coli* cell pellet was resuspended in distilled water (500 µL). The sample was subjected to three repetitions of a temperature incubation step at 95 °C for 10 min, interspersed with short mixing intervals. The denatured insoluble cell components were separated from the soluble fraction by centrifugation (16,000 x g, 20 min, 4 °C). Luria Broth liquid medium (200 µL) supplemented with distilled water (500 µL), which was subjected to the same treatment as the sample, was used as a reference. The conductance and molarity of the soluble fractions were measured with a Mettler Toledo S230 pH/ion meter. The instrument was calibrated with sodium- and potassium-hydrogen-phosphate ion standards and the electrode was a potassium-chloride electrolyte filled probe, such that the data mainly reflect monovalent cation concentrations. The total intracellular salt content was calculated as the molarity difference between the sample and the control after correction for dilution from three independent measurements.

RESULTS AND DISCUSSION

Purification of Li-MreB

The aim of this study was to investigate the *in vitro* biochemical and functional properties of MreB from *Lepstospira interrogans*. Since a purification protocol for *Li*-MreB had not been published, successful procedures that had been applied to MreBs from other species were initially implemented. The soluble expression and purification of *Li*-MreB was problematic. In an attempt to purify *Li*-MreB we employed the protocol established for *Tm*-MreB (8), in which the protein was purified without added nucleotides. In contrast to *Tm*-MreB, *Li*-MreB was irreversibly denatured in the absence of nucleotides, which was reflected by a visible aggregation of the protein solution. Our observations indicate the necessity of bound nucleotide for the structural integrity of *Li*-MreB. Various buffer conditions were tested to avoid the adoption of a denaturation protocol for *Li*-MreB purification, including: calcium (up to 2 mM), potassium (up to 500 mM), magnesium (up to 2 mM) and DTT (up to 10 mM). However, no conditions were found that prevented the denaturation of *Li*-MreB in the absence of nucleotides. Given this requirement for nucleotide all further experiments were carried out in the presence of 0.2 mM ATP. Interestingly, this requirement for ATP also applies to the purification of the monomeric form of eukaryotic actin (20). Subsequently, two strategies were pursued to produce large amounts of functional *Li*-MreB, namely, purification under native conditions and purification with the application of denaturants.

First, the *Li*-MreB expression vector was transformed into BL21 DE3 cells. Induction with IPTG demonstrated robust *Li*-MreB expression (Fig. 1A, lanes 1 and 2). The majority of the *Li*-MreB was found in the pellet (Fig. 1A, lane 2), indicating that *Li*-MreB may be incorporated into inclusion bodies or perhaps forms filaments or other aggregated structures. The *Li*-MreB supernatant was applied to a Ni-NTA column and washed with lysis buffer to reduce the levels of non-specifically bound proteins (Fig. 1A, lane 4 and 5). The His-tagged *Li*-MreB was eluted from the resin with increasing concentrations of imidazole. 50-100 mM imidazole was typically sufficient to elute the majority of *Li*-MreB (Fig. 1A, lanes 6, 7 and 8), while a subpopulation of bound protein remained attached to the column (Fig. 1A, lane 9). This native purification procedure produced a yield of 15-20 mg of soluble *Li*-MreB from a 2 L preparation.

As an alternative to the purification under native conditions, a denaturing preparation protocol for *Li*-MreB was developed. In this protocol the expression protocol for *Li*-MreB was similar to the native conditions preparation, but in contrast, guanidine-HCl (6 M) was added to

the cells prior to centrifugation. The supernatant, containing the solubilized and presumably unfolded *Li*-MreB, was loaded onto a Ni-NTA column. After overnight incubation the column was washed with a buffer containing 8 M urea. The pH of the buffer was gradually decreased from pH 8.0 to pH 4.0. The largest amount of *Li*-MreB eluted from the column at pH 7.0 (Fig. 1B, lane 2, 4). The peak fractions were combined and the refolding of *Li*-MreB was promoted by gel filtration against non-denaturing buffer (buffer A). This denaturation preparation method yielded ~ 50 mg of *Li*-MreB from a 2 L culture, which is approximately three times more than achieved using the native conditions protocol. These observations demonstrate that *Li*-MreB can be purified in greater quantities under denaturing conditions than under native conditions.

The salt concentration in bacteria

To confirm the physiologically relevant salt concentration range in bacteria prior to undertaking *Li*-MreB assembly experiments, we estimated the ionic strength within bacterial cells. An *E. coli* cell pellet was resuspended and then boiled in distilled water. The denatured cell components were separated from the soluble fraction by centrifugation. The control sample was LB liquid medium, which was treated in an identical manner to the *E. coli* sample. The conductance and molarity in each supernatant was measured. The difference of the salt content between the sample and control was assumed to reflect the cytoplasmic salt concentrations of the bacteria, which was measured to be 326 ± 14 mM total monovalent salt. Although this value may vary between bacteria species and can also depend on the state of the cells, the results confirm that the ionic strength is much greater in bacterial cells than in eukaryotic cells, and falls into the range of several hundreds of mM. This observation is in agreement with previous measurements (24).

Functional characterization of Li-MreB

After the method of purification was established, the purified proteins were tested in *Li*-MreB assembly assays. *Li*-MreB assembly was initially monitored by following the increase in light scattering for both the renatured and native purified *Li*-MreBs. The polymerisation of MreB from other species has been reported to be initiated by the addition of nucleotides. In our experiments the *Li*-MreB solution contained 0.2 mM ATP and the light scattering signal did

not change after the addition of further ATP (2 mM). In contrast, the assembly of *Li*-MreB could be initiated by the addition of magnesium (2 mM $MgCl_2$) and / or by elevating the ionic strength with the addition of KCl. When KCl (100 mM) and $MgCl_2$ (2 mM) were added to the protein solution the light scattering increased indicated the assembly of *Li*-MreB. Similar tendencies were observed for native and renatured *Li*-MreB (data are not shown), suggesting that the renatured *Li*-MreB was functional and properly refolded into its native structure.

We next investigated the buffer conditions that could modify the assembly properties of *Li*-MreB. When the polymerization of *Li*-MreB was monitored in the presence of constant $MgCl_2$ (2 mM) over a range of KCl concentrations (0-500 mM), the *Li*-MreB assembly-induced increase of the light scattering showed strong ionic strength dependence (Fig. 2A). At KCl concentrations above 400 mM the extent of assembly of *Li*-MreB was small and the rate of assembly was slow ($k_{obs} = 10^{-4}$ s^{-1}) (Fig. 2B). However, between 100 and 400 mM KCl the intensity of the scattered light was increased during the polymerization of *Li*-MreB reaching its maximum value at 300 mM KCl (Fig. 2C). At this KCl concentration the assembly was accelerated to 7×10^{-4} s^{-1} (Fig. 2B). This tendency of salt dependent assembly of *Li*-MreB differs from that observed previously for *E. coli* MreB (*Ec*-MreB) in low salt conditions, but shows good agreement at high KCl concentrations (17).

Thus, the fastest assembly of *Li*-MreB occurs at approximately 200-300 mM KCl concentrations. This concentration range coincides with the ionic strength that we measured in bacterial cells, suggesting that the structural and biochemical properties of *Li*-MreB are optimised for the ionic conditions manifested in living cells.

Next we tested the effects of magnesium on the assembly of *Li*-MreB. In these experiments the KCl concentration was constant (200 mM) and the concentration of magnesium was varied (0-8 mM). The change of the light scattering signal was the largest in the absence of magnesium (Fig. 3A, B). After the addition of $MgCl_2$ the amplitude of the signal changes became smaller. At 2 mM $MgCl_2$ the changes began to level out and showed only small further variations at greater magnesium concentrations (Fig. 3C). The rates of assembly calculated from the light scattering changes were independent of the $MgCl_2$ concentration (7×10^{-4} s^{-1}) (Fig. 3B). In separate experiments, we observed that the addition of calcium (4 mM) also induced *Li*-MreB assembly. In the absence of KCl, the addition of 4 mM $CaCl_2$ produced a larger increase in light scattering than observed for the addition of 4 mM $MgCl_2$. Thus, the increase in the light scattering resulting from *Li*-MreB assembly in response divalent ions, calcium or magnesium,

was greater in the absence of monovalent salts. Figure 4 summarises the observations. These data suggest that the degree or type of *Li*-MreB assembly can vary under different salt conditions.

Li-MreB assembly monitored by sedimentation

To confirm the observations from the light scattering experiments the assembly of *Li*-MreB was further characterised by sedimentation studies. *Li*-MreB (50 μM) was incubated overnight at 4 ^{o}C in the presence of various concentrations of KCl, $MgCl_2$ and nucleotides (ATP or ADP). After ultracentrifugation (100,000 x g at 4 ^{o}C for 30 min) the pellet from each sample was analysed using 10 % SDS-PAGE gels (Fig. 5). Under these conditions *Li*-MreB sedimented and the quantities of *Li*-MreB observed in the pellets were dependent on buffer conditions. In the presence of 0.2 mM ATP a moderate level of *Li*-MreB sedimentation was detected (Fig. 5, lane 2). In the presence of a ten-fold increase of ATP (2 mM) there was a slight increase in the amount of pelleted *Li*-MreB, which was not observed for ADP (Fig. 5, lanes 3 and 4), indicating that increased concentrations of ATP play a small role in the regulation of *Li*-MreB assembly. When potassium (100 mM) and magnesium (2 mM) were added, the levels of *Li*-MreB sedimentation were substantially increased (Fig. 5, lanes 5, 8 and 11).

Thus, the results from the light scattering and sedimentation experiments show that although the presence of ATP (or other nucleotides) is essential for the function of *Li*-MreB, higher concentrations of nucleotides have little additional effect on the assembly properties. This behaviour is in contrast to the MreB from other species, in which ATP concentrations are added to induce polymerization (8, 14). The kinetics and extent of *Li*-MreB assembly are strongly depended on the salt conditions. Both the nature and concentration of added salts (KCl, $MgCl_2$, $CaCl_2$) were important in defining the assembly of *Li*-MreB. An explanation for these observations may be that the critical concentration for *Li*-MreB assembly, and / or the filament oligomerisation state, depends on the salt conditions. Light scattering and sedimentation studies are insensitive to protein assembly morphologies, since these techniques do not clearly distinguish between polymerisation, formation of other suprastructures, or precipitation. Hence, we chose to further monitor *Li*-MreB filament formation by fluorescence.

Li-MreB assembly monitored by fluorescence

We labelled the *Li*-MreB with an extrinsic fluorophore in order to have a more specific method to monitor polymerization. We targeted the two native cysteine residues (Cys^{314} and Cys^{340}) of *Li*-MreB for this process using Alexa 488-maleimide. The labelling was carried out by incubating the protein with the fluorophore and then by removing the free dye by gel filtration. Photometric measurements showed that the probe bound to *Li*-MreB with an estimated labelling ratio of ~ 50 % (1 label to 2 *Li*-MreBs). To determine which amino acids reacted with the Alexa 488-maleimide, we carried out mass spectrometry analysis, which identified that both cysteine residues were capable of forming adducts with the fluorophore. Since a 3D crystal structure is not yet available for *Li*-MreB, the structure of *Tm*-MreB was used to model the positions of the reactive cysteines (Fig. 6). The *Tm*-MreB structure suggests that both *Li*-MreB cysteine residues lie close to the nucleotide-binding cleft.

The fluorescence intensity of the *Li*-MreB-bound Alexa 488-maleimide was initially characterized and proved to be stable in the absence of assembly-promoting agents (Fig. 7A). On initiation of polymerization by the addition of salts, the fluorescence intensity from the Alexa 488-maleimide decreased (Fig. 7A). This observation indicates that the labelling did not interfere significantly with the assembly properties of *Li*-MreB. The decrease of fluorescence signal may be attributed to an increase in fluorescence quenching that was enhanced by the relocation of the functional groups around the fluorophore during assembly.

The analysis of these transitions revealed that when *Li*-MreB (50 μM) was assembled in the presence of 10 mM KCl and 0.5 mM $MgCl_2$ the intensity change was approximately 25 % (Fig. 7A). Increasing the salt concentrations (100 mM KCl and 2 mM $MgCl_2$) resulted in larger intensity decreases (approximately 45 %). The experiments were then repeated with various *Li*-MreB concentrations between 5 and 50 μM and the changes in the fluorescence intensity were plotted as the function of the protein concentration (Fig. 7B). The fluorescence intensity decreases were larger at greater potassium and magnesium concentrations. Figure 7B also shows that although the amplitude of change is smaller in the presence of low salt concentration, it levels off at lower *Li*-MreB concentrations. To describe the kinetics of assembly, exponential curves were fitted to the data and the apparent rate constants were determined (Fig. 7C). The MreB concentration dependence of the rate constant indicates that MreB can assemble faster at higher concentrations. The assembly was also faster at lower KCl concentrations. This is in good agreement with previous results obtained for *Ec*-MreB (17).

The curves show a fast initial drop followed by a gentle decrease in fluorescence. We analysed this initial rapid phases in stopped flow experiments. *Li*-MreB-Alexa488 was mixed with buffers containing salts at various concentrations to initiate *Li*-MreB assembly. The initial transitions were analysed by applying single exponential models. The obtained rate constants were independent of the applied concentrations of *Li*-MreB (5 and 50 μM) and gave an average value of $13.1 \pm 2.7\ s^{-1}$. We concluded that the first rapid step of MreB assembly describes a conformational change in *Li*-MreB that is a first order reaction. Interestingly, the ionic conditions beyond 10 mM KCl and 0.5 mM $MgCl_2$ did not influence the rate of the first step of association (Fig. 7D). Accordingly, these data suggest that *Li*-MreB assembly is at least a two-step process, with the second step of *Li*-MreB assembly being observed in the steady-state fluorescence experiments (Fig. 7A). While the first step is mostly independent of the environmental parameters, the second step is sensitive to the concentration and nature of the salts.

We attempted to characterise the disassembly of *Li*-MreB in experiments where polymerised Alexa-488-maleimide labelled *Li*-MreB was diluted to different concentrations under non-polymerisation (buffer A) or polymerisation (buffer A + 2 mM $MgCl_2$ and 100 mM KCl) conditions. On dilution, the intensity of the fluorescence signal increased (Fig. 8A). Since, *Li*-MreB assembly results in a decrease of fluorescence signal, we interpret the increase in the fluorescence signal as the signal for the disassembly of *Li*-MreB. The disassembly rate of *Li*-MreB depended on ionic conditions (Fig. 8A). Sedimentation-based analysis of disassembly was also carried out. Polymerised *Li*-MreB was diluted under polymerisation (buffer A + 2 mM $MgCl_2$ and 100 mM KCl) or non-polymerisation (buffer A) conditions and the samples were incubated overnight at 4 ^{o}C before sedimentation. Under non-polymerisation conditions the disassembly of *Li*-MreB was more pronounced than in the presence of magnesium and potassium ions (Fig. 8B). Considering that the samples were incubated for long time periods for the sedimentation studies, these data likely represent the equilibrium between the assembled and monomeric *Li*-MreB populations that were established under the various conditions. The difference between the amounts of *Li*-MreB measured in the pellets likely reflects the changes in the critical concentration for assembly under the various conditions.

Filament assembly observed by fluorescence microscopy

The ionic strength-dependent light scattering and fluorescence spectroscopic data indicate that *Li*-MreB may form supramolecular complexes under polymerisation conditions. To visualise these assemblies formed by *Li*-MreB, we applied *in vitro* fluorescence microscopy. Alexa-488-maleimide-labelled *Li*-MreB was imaged on the surface of glass slides. Speckle-like short oligomers of *Li*-MreB with different lengths appeared in buffer A (Fig. 9A), indicating that pure monomeric solution of *Li*-MreB is difficult to achieve under these conditions. Note, that in the cases of MreB from other species monomeric solutions were obtained by eliminating the nucleotides from the buffers. In the case of *Li*-MreB, it was not possible due to the denaturation of *Li*-MreB. When the fluorescence images were recorded for samples supplemented with 100 mM KCl and 2 mM $MgCl_2$ the *Li*-MreB filaments were much longer, typically as long as 20-100 μm. These filaments self-associated into bundles and sheet-like structures (Fig. 9B). The sheet-like structures appeared to roll up forming bundles (Fig. 9B), but narrow bundles could be observed in the presence of salt (Fig. 9C). On the addition of 4 mM $CaCl_2$ in the absence of KCl (Fig. 9C), these structures varied significantly from those that were observed in the presence of $MgCl_2$ and KCl (Fig. 9D). We suggest that the KCl dependent differences in the light scattering intensities in the spectroscopic experiments (Fig. 2 and Fig. 7) reflect the variation of the assemblies observed in the microscopic images.

These fluorescence images demonstrate that *Li*-MreB forms various polymeric structures under different buffer conditions (Fig. 9). The *Li*-MreB filaments and bundles often display bent, curled or helical morphologies. These structures can be classified into different groups. The appearance of short filaments or oligomers under low ionic strength conditions (in buffer A) is in good agreement with the small amount of *Li*-MreB found in the pellet of sedimentation assay (Fig. 5). The filaments, thick cables and filament networks observed in the presence of 2 mM $MgCl_2$ and 100 mM KCl are consistent with enhanced sedimentation (Fig. 5). The $CaCl_2$-induced assemblies in the absence of KCl (Fig. 4) resemble the *B. subtilis* MreB polymer structures observed in the presence of $MgCl_2$ (25). We speculate that the oligomer association prior to the polymerisation must be fast, since the process of assembly was too fast to be captured in the microscope experiments.

CONCLUSIONS

We have established a biochemical preparation method with which yields a 3-fold increase in purified *Li*-MreB over existing methods to purify MreBs. The protein is functional as evidenced by its ability to form assemblies and to bind ATP. We have demonstrated that the assembly of *Li*-MreB is sensitive to ionic conditions, and the rate of *Li*-MreB assembly shows a maximum around 300 mM KCl (Fig. 2C, lower panel), which approximates to the measured bacterial *in vivo* salt concentration.

The *Li*-MreB was successfully labelled with an extrinsic fluorophore to probe the complex mechanisms contributing to the assembly. The fluorophore was sub-stochiometrically attached to two cysteines that lie in the nucleotide-binding cleft. The sum fluorescence signal proved to be sensitive to the dynamics of *Li*-MreB. This fluorescence intensity decreased during the assembly of *Li*-MreB in two steps. The first fast step was not seen in the light scattering experiments and we attribute this to a conformational transition within the *Li*-MreB monomers. The second step is the formation of *Li*-MreB filaments and other suprastructures of *Li*-MreB.

In the first step, the intensity declined very quickly in approximately 100 ms. The rate constant characteristic for the first step did not depend on the concentration of *Li*-MreB, which indicates that it is a first-order reaction. The fluorescent probe appears to be sensitive to conformational switching within *Li*-MreB, and as a consequence the probe serves as a useful tool in the investigation of the polymerisation and depolymerisation properties of *Li*-MreB. The two major domains of eukaryotic actin are known to rotate during the actin polymerisation, which result in changes at the nucleotide binding site and presumably activate the ATPase activity (26–30). Molecular dynamics simulations support to hypothesis that similar conformational changes for *Tm*-MreB (31). Based on this interpretation we hypothesize that the fast change of the fluorescence signal is caused by a conformational change in the protomer, which changes the environment of the fluorophores. Further perturbations in this environment occur during the slower process of filament assembly and the reverse process is observed on filament disassembly. Thus, the fluorescence probe is a sensitive and selective reporter for the *Li*-MreB protomer conformation, and is also sensitive to the slower process of filament formation, which is highly salt concentration dependant.

Since, the labelling did not appear to perturb the polymerization properties of *Li*-MreB, the fluorescently labelled *Li*-MreB is useful for visualisation of filaments in the fluorescence microscope. The resultant images demonstrate that *Li*-MreB filaments can interact with each

other to form large supramolecular complexes, such as sheets and bundles, which were dependent on assembly conditions. We conclude that *Li*-MreB can behave as a versatile component of bacterial cell wall coordinating machinery and the nature of its self-organisation serves as the basis of the integrity and function of the underlying protein system. We suggest that the observed self-assembly of *Li*-MreB will play a central role in the biological function of this actin-like bacterial protein. Considering that in living bacteria MreB networks function to fulfil a structural and dynamic role in organising cell wall synthesis, detailed investigation of the properties of these suprafilamental structures and the identification of the partner proteins regulating their changes will be important in future experiments. The methods of *Li*-MreB preparation and visualisation described here will be useful tools in the further characterisation of these molecular processes.

LEGENDS TO FIGURES

Figure 1.: Purification of Li-MreB. **(A)** Purification of *Li*-MreB under native conditions on Ni-NTA resin as analysed by SDS-PAGE. The pellet obtained after cell lysis contained the majority of the overexpressed *Li*-MreB (lane 2) with a minor amount of *Li*-MreB appearing in the clarified soluble fraction (lane 1). The Ni-NTA column was washed with 5 mM and 10 mM imidazole (lanes 4 and 5). *Li*-MreB was eluted with a stepwise gradient of 50 mM, 100 mM and 350 mM imidazole (lane 6, 7 and 8). A fraction of the *Li*-MreB, along with impurities, remained bound to the resin, which were subsequently eluted by SDS. **(B)** Purification of *Li*-MreB on Ni-NTA resin under denaturing conditions. Denatured *Li*-MreB in 8 M urea was eluted by a pH gradient: pH 8.0 (lane 1), pH 7.0 (lane 2) and pH 6.0 (lane 4), while the majority of the contaminants remained bound to the resin (lane 7). Sliced parts of the same gels are separated by narrow white spaces for clarity.

Figure 2.: KCl dependent assembly of Li-MreB. **(A)** Light scattering assay following the assembly of 30 μM *Li*-MreB initiated by the addition of 2 mM $MgCl_2$ and various concentrations of KCl (black line: 100 mM, red: 200 mm, green: 300 mM and orange: 500 mM). **(B)** The rates of assembly obtained by using single exponential fits. **(C)** The relative change in the light scattering signal as the function of the KCl concentration.

Figure 3.: Magnesium dependent assembly of Li-MreB. **(A)** Light scattering assay following the assembly of 30 μM *Li*-MreB initiated by the addition of 200 mM KCl and various concentrations of $MgCl_2$ (black line: 0 mM, red 4 mM and blue: 8 mM). The observed rates **(B)** and the relative changes **(C)** in the transients are presented as the function of the magnesium concentration.

Figure 4.: Salt and cation dependent assembly of Li-MreB. **(A)** Rates of assembly (**B)** light scattering of 30 μM *Li*-MreB assembly in the presence of KCl, $MgCl_2$ or $CaCl_2$.

Figure 5.: Sedimentation of polymerised Li-MreB. *Li*-MreB was assembled under various conditions at different ATP, ADP, KCl, and $MgCl_2$ concentrations (as indicated in the figure) and then sedimented by ultracentrifugation. The pellets were analysed by SDS-PAGE and presented in the figure.

Figure 6.: The positions of the two cysteines in the model of Li-MreB. Sequence alignment of MreBs predicts that *Li*-MreB Cys^{294} and Cys^{320} will be at equivalent positions to Ser^{288} and Ala^{314} of *Tm*-MreB. Both residues are localized in the nucleotide-binding cleft.

Figure 7.: Li-MreB assembly revealed by fluorescence experiments. **(A)** 50 μM Alexa 488 labelled *Li*-MreB was assembled under low (0.5 mM $MgCl_2$, 10 mM KCl; red curve) or high (2 mM $MgCl_2$, 100 mM KCl; blue curve) salt conditions and monitored by fluorescence. The control (black curve) represents the addition of only buffer A. **(B)** The *Li*-MreB concentration dependence of the fluorescence change obtained under low (0.5 mM $MgCl_2$, 10 mM KCl, filled circles) or high salt (2 mM $MgCl_2$, 100 mM KCl; open squares) conditions. **(C)** The observed rates were obtained by using single exponential fits. The data are presented from experiments at various salt conditions. Filled circles: 10 mM KCl, 0.5 mM $MgCl_2$; filled squares: 100 mM KCl, 2 mM $MgCl_2$; and open circles: 350 mM KCl, 4 mM $MgCl_2$. **(D)** Stopped-flow fluorescence data from the initial phase of the assembly of *Li*-MreB as observed under various salt conditions (black line: 10 mM KCl, 0.5 mM $MgCl_2$, blue: 100 mM KCl, 2 mM $MgCl_2$, red: 350 mM KCl, 4 mM $MgCl_2$).

Figure 8.: The disassembly of Li-MreB. ***(A)*** Fluorescence changes resulting from 25 μM Alexa 488 maleimide labelled *Li*-MreB on dilution to 2 μM with buffer A (black curve) or polymerisation buffer (red curve). ***(B)*** Sedimentation data where 25 μM *Li*-MreB was first polymerised and then diluted to the various concentrations indicated in polymerisation (2 mM $MgCl_2$, 100 mM KCl) or non-polymerisation (buffer A) conditions.

Figure 9. Li-MreB forms salt dependent bundles. Fluorescence microscope images (bar 20 μm). **(A)** The *Li*-MreB-Alexa488 stock (20 μM) in buffer A shows speckles which may represent small oligomers of different lengths. **(B-C)** Under high salt conditions (2 mM $MgCl_2$, 100 mM KCl) large sheets (B) and bundles (C) are observed. **(D)** Lace-like *Li*-MreB polymers were formed in the presence of 4 mM $CaCl_2$.

ACKNOWLEDGEMENT

This study was supported by grants from the Hungarian Science Foundation (OTKA) NN107776 and K112794 (to MNy), grants from the Hungarian National Office for Research and Technology (GVOP-3.2.1.-2004-04-0190/3.0 and GVOP-3.2.1.-2004-04-0228/3.0 (to MNy)) and by the Grant of PTE ÁOK-KA-2013/1 (to GH). This work was also supported by 'Science, Please! Research Team on Innovation' (SROP-4.2.2/08/1/2008-0011) program and by the European Union and the State of Hungary, co-financed by the European Social Fund in the framework of TÁMOP-4.2.4.A/ 2-11/1-2012-0001 'National Excellence Program'.
D.P and R.C.R are supported by the Agency for Science, Technology and Research (A*STAR), Singapore. The present scientific contribution is dedicated to the 650th anniversary of the foundation of the University of Pécs, Hungary.

REFERENCES

1. Mirouze, N., C. Ferret, Z. Yao, A. Chastanet, and R. Carballido-López. 2015. MreB-Dependent Inhibition of Cell Elongation during the Escape from Competence in Bacillus subtilis. PLOS Genet. 11: e1005299.

2. Rojas, E., J. a Theriot, and K.C. Huang. 2014. Response of Escherichia coli growth rate to osmotic shock. Proc. Natl. Acad. Sci. U. S. A. 111: 7807–12.

3. Amir, A., and S. van Teeffelen. 2014. Getting into shape: How do rod-like bacteria control their geometry? Syst. Synth. Biol. : 227–235.

4. Figge, R.M., A. V. Divakaruni, and J.W. Gober. 2004. MreB, the cell shape-determining bacterial actin homologue, co-ordinates cell wall morphogenesis in Caulobacter crescentus. Mol. Microbiol. 51: 1321–1332.

5. Gitai, Z., N.A. Dye, A. Reisenauer, M. Wachi, and L. Shapiro. 2005. MreB actin-mediated segregation of a specific region of a bacterial chromosome. Cell. 120: 329–41.

6. Dye, N.A., Z. Pincus, J.A. Theriot, L. Shapiro, and Z. Gitai. 2005. Two independent spiral structures control cell shape in Caulobacter. Proc. Natl. Acad. Sci. U. S. A. 102: 18608–13.

7. Wang, S., H. Arellano-Santoyo, P.A. Combs, and J.W. Shaevitz. 2010. Actin-like cytoskeleton filaments contribute to cell mechanics in bacteria. Proc. Natl. Acad. Sci. U. S. A. 107: 9182–5.

8. van den Ent, F., L. a Amos, and J. Löwe. 2001. Prokaryotic origin of the actin cytoskeleton. Nature. 413: 39–44.

9. Van den Ent, F., J. Møller-Jensen, L. a. Amos, K. Gerdes, and J. Löwe. 2002. F-actin-like filaments formed by plasmid segregation protein ParM. EMBO J. 21: 6935–6943.

10. Gayathri, P., T. Fujii, K. Namba, and J. Löwe. 2013. Structure of the ParM filament at 8.5Å resolution. J. Struct. Biol. 184: 33–42.

11. Popp, D., A. Narita, T. Oda, T. Fujisawa, H. Matsuo, Y. Nitanai, M. Iwasa, K. Maeda, H. Onishi, and Y. Maéda. 2008. Molecular structure of the ParM polymer and the mechanism leading to its nucleotide-driven dynamic instability. EMBO J. 27: 570–9.

12. van den Ent, F., T. Izoré, T.A. Bharat, C.M. Johnson, and J. Löwe. 2014. Bacterial actin

MreB forms antiparallel double filaments. Elife. 3: e02634.

13. Popp, D., A. Narita, K. Maeda, T. Fujisawa, U. Ghoshdastider, M. Iwasa, Y. Maéda, and R.C. Robinson. 2010. Filament structure, organization, and dynamics in MreB sheets. J. Biol. Chem. 285: 15858–65.

14. Esue, O., M. Cordero, D. Wirtz, and Y. Tseng. 2005. The assembly of MreB, a prokaryotic homolog of actin. J. Biol. Chem. 280: 2628–35.

15. Nurse, P., and K.J. Marians. 2013. Purification and characterization of Escherichia coli MreB protein. J. Biol. Chem. 288: 3469–75.

16. Daniel, R.A., and J. Errington. 2003. Control of Cell Morphogenesis in Bacteria. Cell. 113: 767–776.

17. Domínguez-Escobar, J., A. Chastanet, A.H. Crevenna, V. Fromion, R. Wedlich-Söldner, and R. Carballido-López. 2011. Processive movement of MreB-associated cell wall biosynthetic complexes in bacteria. Science. 333: 225–8.

18. Garner, E.C., R. Bernard, W. Wang, X. Zhuang, D.Z. Rudner, and T. Mitchison. 2011. Coupled, circumferential motions of the cell wall synthesis machinery and MreB filaments in B. subtilis. Science. 333: 222–5.

19. Mcbride, A.J.A., D.A. Athanazio, M.G. Reis, and A.I. Ko. Leptospirosis. : 376–386.

20. Slamti, L., M. a. de Pedro, E. Guichet, and M. Picardeau. 2011. Deciphering Morphological determinants of the helix-shaped Leptospira. J. Bacteriol. 193: 6266–6275.

21. Cayley, S., B.A. Lewis, H.J. Guttman, and M.T. Record. 1991. Characterization of the cytoplasm of Escherichia coli K-12 as a function of external osmolarity. J. Mol. Biol. 222: 281–300.

22. Defeu Soufo, H.J., C. Reimold, H. Breddermann, H.G. Mannherz, and P.L. Graumann. 2015. Translation elongation factor EF-Tu modulates filament formation of actin-like MreB protein in vitro. J. Mol. Biol. 427: 1715–1727.

23. Pfaendtner, J., D. Branduardi, M. Parrinello, T.D. Pollard, and G. a Voth. 2009. Nucleotide-dependent conformational states of actin. Proc. Natl. Acad. Sci. U. S. A. 106: 12723–12728.

24. Zheng, X., K. Diraviyam, and D. Sept. 2007. Nucleotide effects on the structure and

dynamics of actin. Biophys. J. 93: 1277–1283.

25. Graceffa, P., and R. Dominguez. 2003. Crystal structure of monomeric actin in the ATP state: Structural basis of nucleotide-dependent actin dynamics. J. Biol. Chem. 278: 34172–34180.

26. Belmont, L.D., a Orlova, D.G. Drubin, and E.H. Egelman. 1999. A change in actin conformation associated with filament instability after Pi release. Proc. Natl. Acad. Sci. U. S. A. 96: 29–34.

27. Oda, T., M. Iwasa, T. Aihara, Y. Maéda, and A. Narita. 2009. The nature of the globular- to fibrous-actin transition. Nature. 457: 441–445.

28. Colavin, A., J. Hsin, and K.C. Huang. 2014. Effects of polymerization and nucleotide identity on the conformational dynamics of the bacterial actin homolog MreB. Proc. Natl. Acad. Sci. U. S. A. 111: 3585–90.

FIGURES

Figure 1.

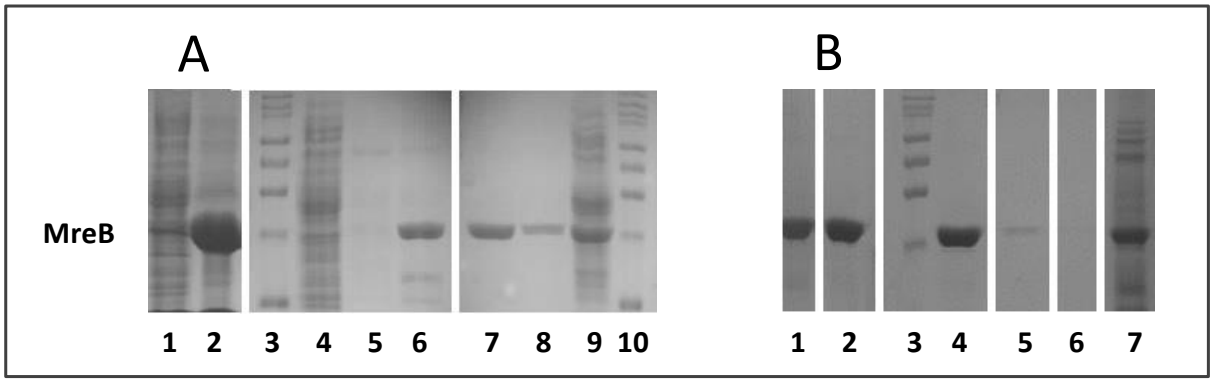

Figure 2.

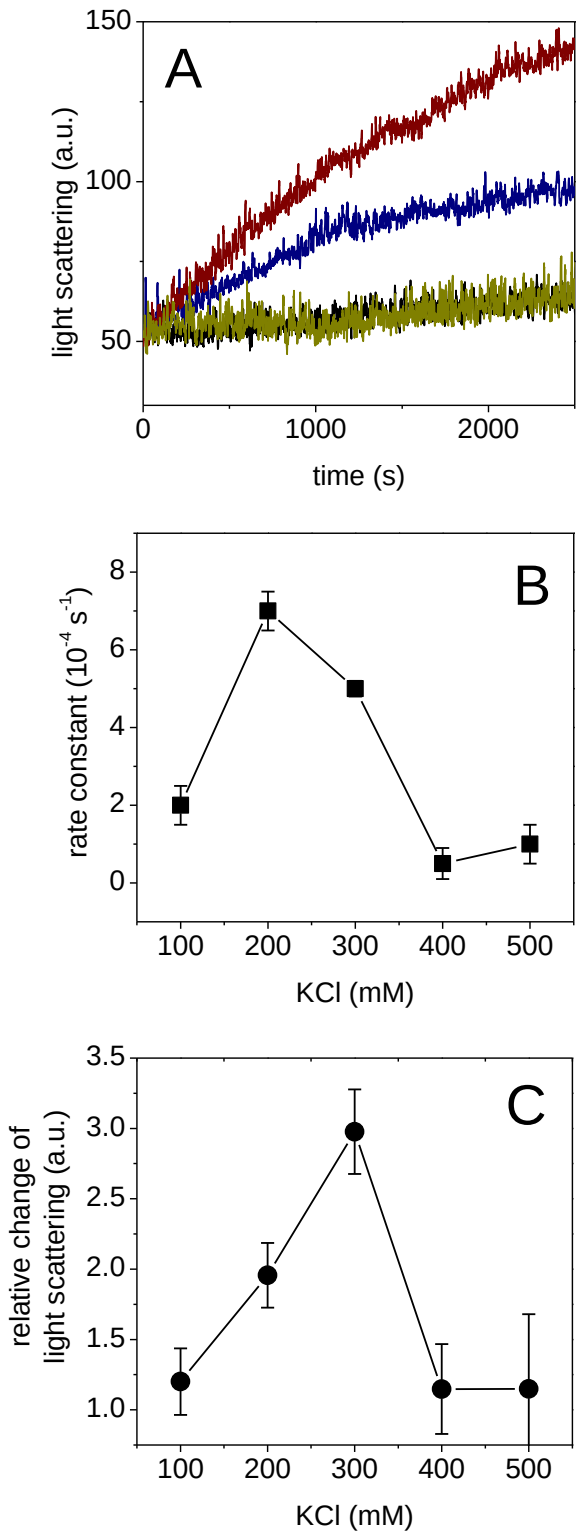
A
light scattering (a.u.)
150
100
50
0
1000
2000
time (s)
B
rate constant (10^{-4} s^{-1})
8
6
4
2
0
100
200
300
400
500
KCl (mM)
C
relative change of light scattering (a.u.)
3.5
3.0
2.5
2.0
1.5
1.0
100
200
300
400
500
KCl (mM)

Figure 3.

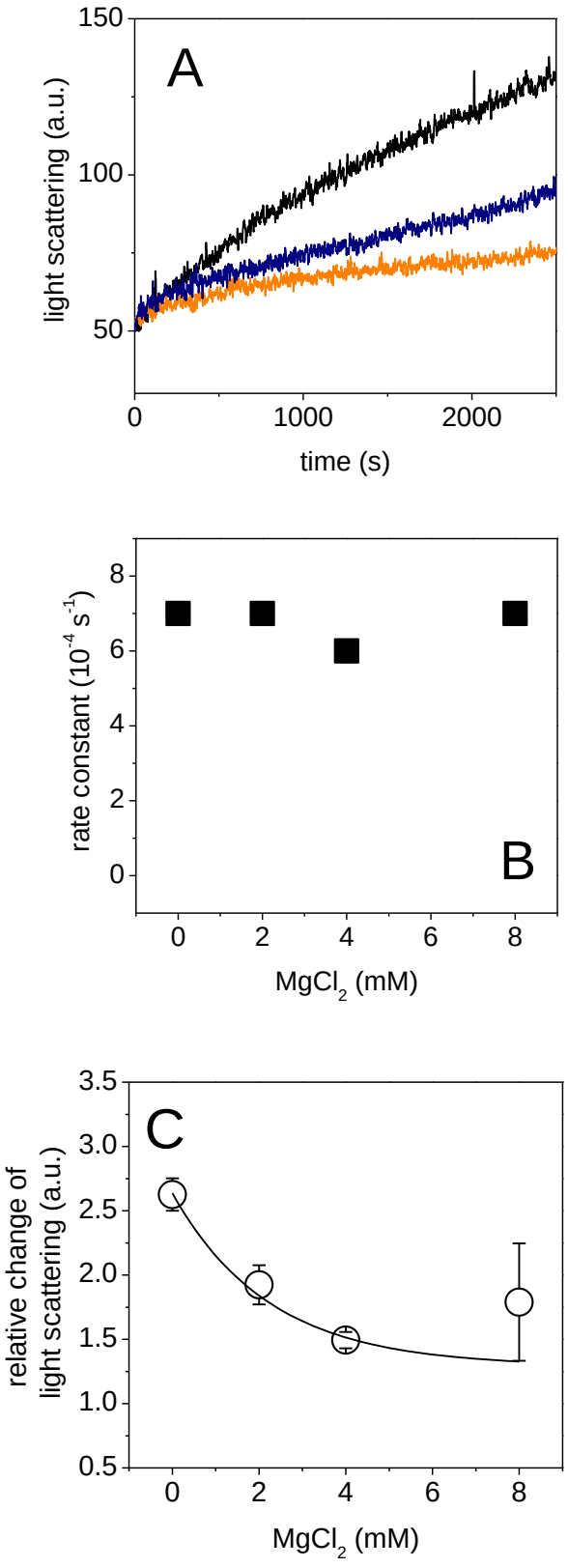
A
light scattering (a.u.)
150
100
50
0
1000
2000
time (s)
B
rate constant (10^{-4} s^{-1})
8
6
4
2
0
0
2
4
6
8
$MgCl_2$ (mM)
C
relative change of light scattering (a.u.)
3.5
3.0
2.5
2.0
1.5
1.0
0.5
0
2
4
6
8
$MgCl_2$ (mM)

Figure 4.

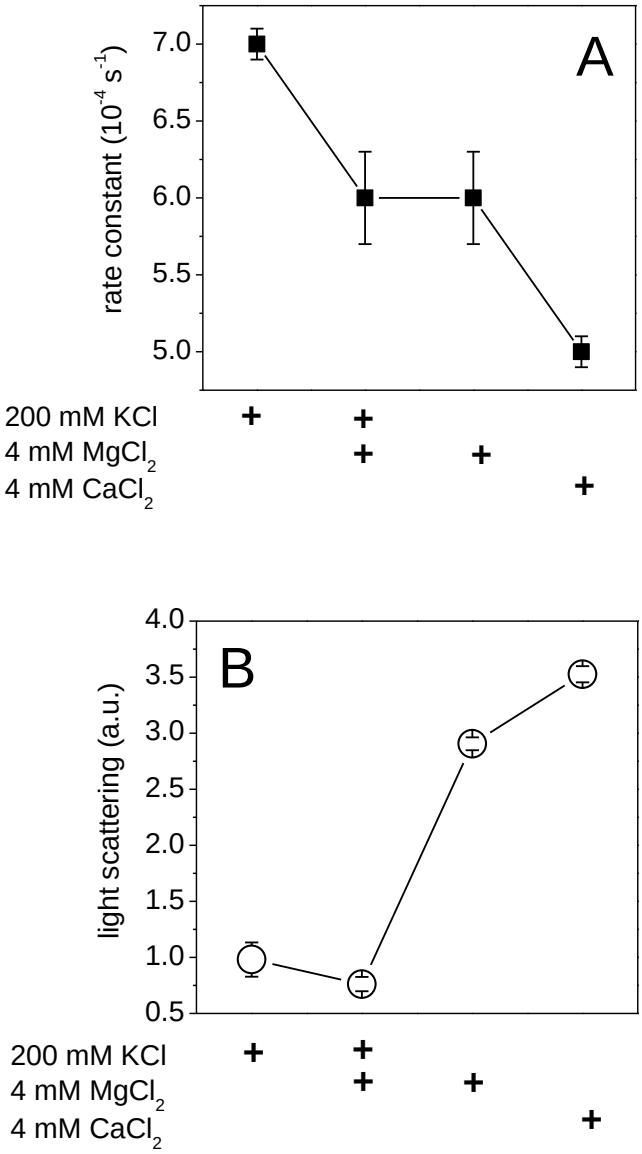
A
rate constant (10^{-4} s^{-1})
7.0
6.5
6.0
5.5
5.0
200 mM KCl
4 mM $MgCl_2$
4 mM $CaCl_2$
B
light scattering (a.u.)
4.0
3.5
3.0
2.5
2.0
1.5
1.0
0.5
200 mM KCl
4 mM $MgCl_2$
4 mM $CaCl_2$

Figure 5.

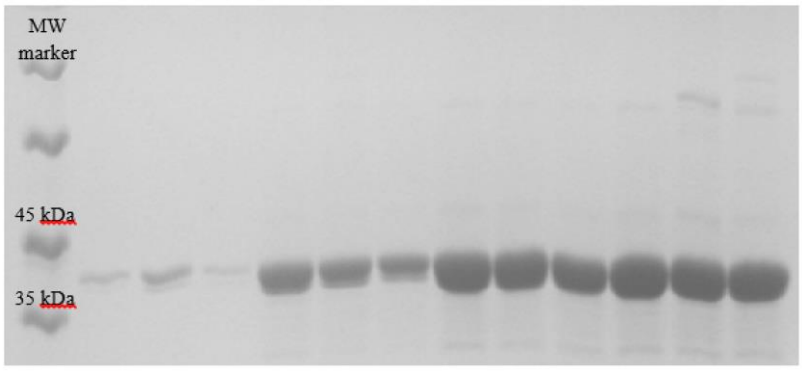

	1	2	3	4	5	6	7	8	9	10	11	12
ATP (mM)	0.2	2.2	0.2	0.2	2.2	0.2	0.2	2.2	0.2	0.2	2.2	0.2
ADP (mM)	0	0	2	0	0	2	0	0	2	0	0	2
KCl (mM)	0	0	0	10	10	10	50	50	50	100	100	100
$MgCl_2$ (mM)	0	0	0	0.5	0.5	0.5	1	1	1	2	2	2

Figure 6.

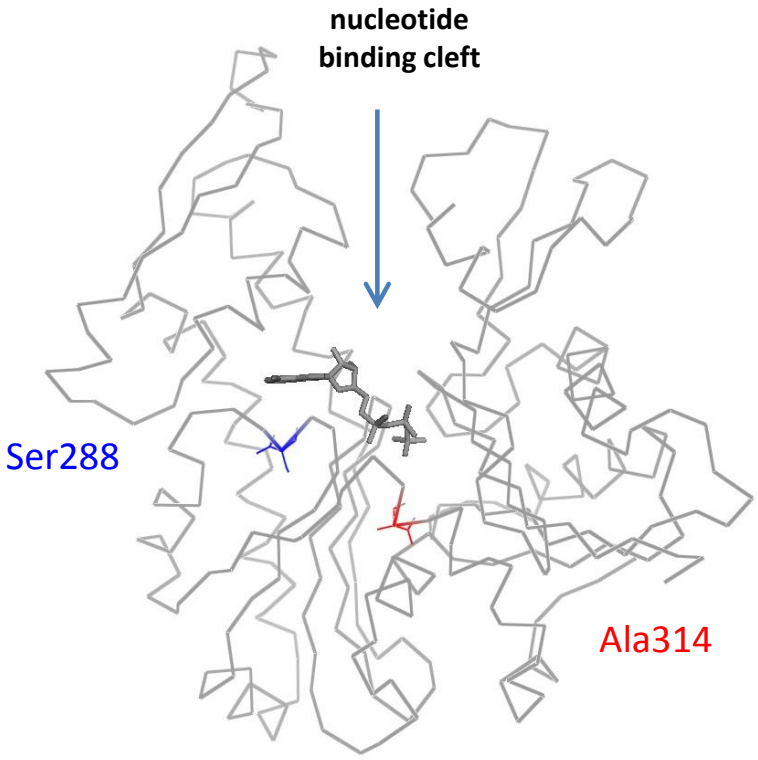

Figure 7.

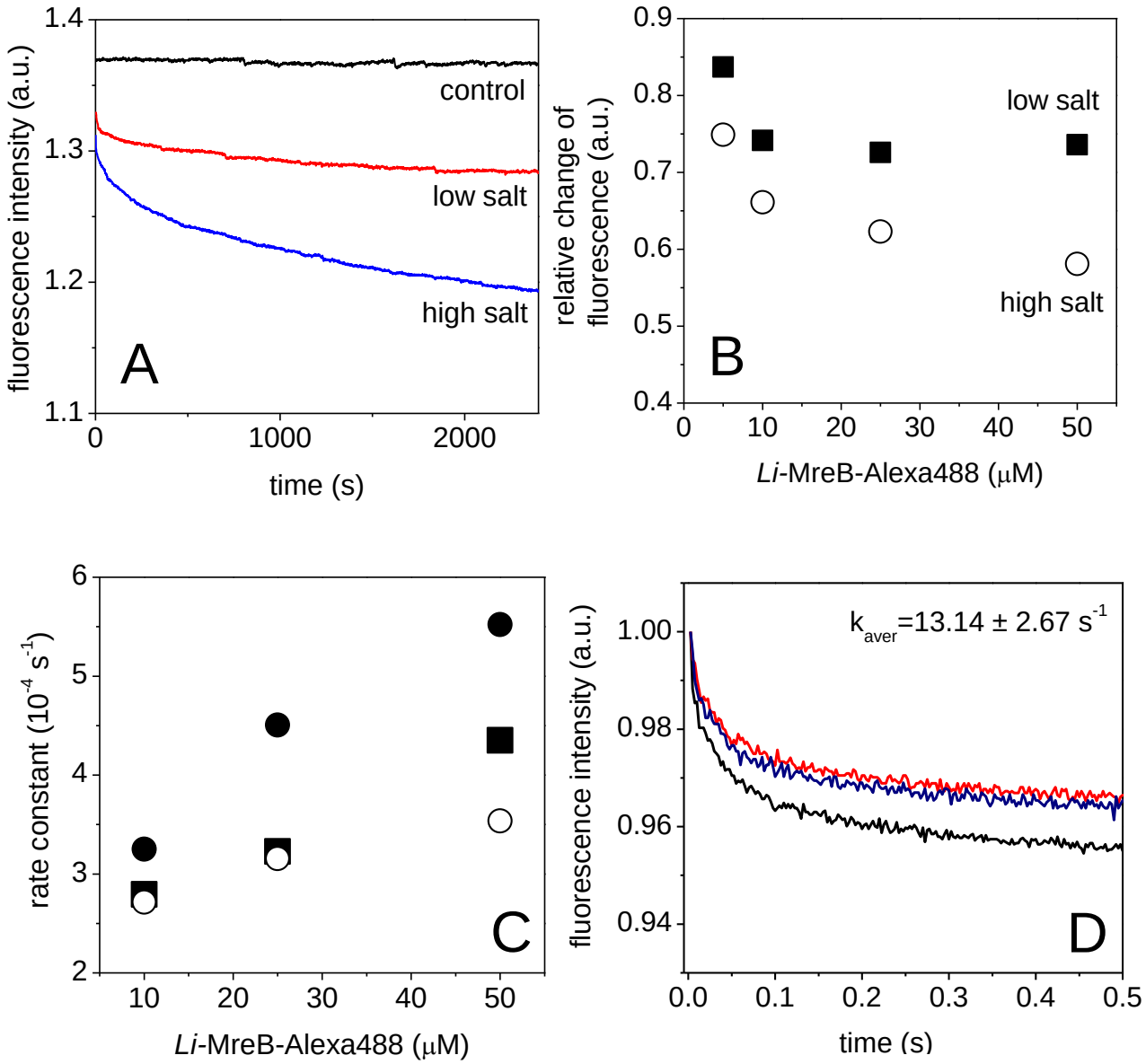
A
fluorescence intensity (a.u.)
time (s)
control
low salt
high salt
B
relative change of fluorescence (a.u.)
Li-MreB-Alexa488 (μM)
low salt
high salt
C
rate constant (10-4 s-1)
Li-MreB-Alexa488 (μM)
D
fluorescence intensity (a.u.)
time (s)
kaver=13.14 ± 2.67 s-1

Figure 8.

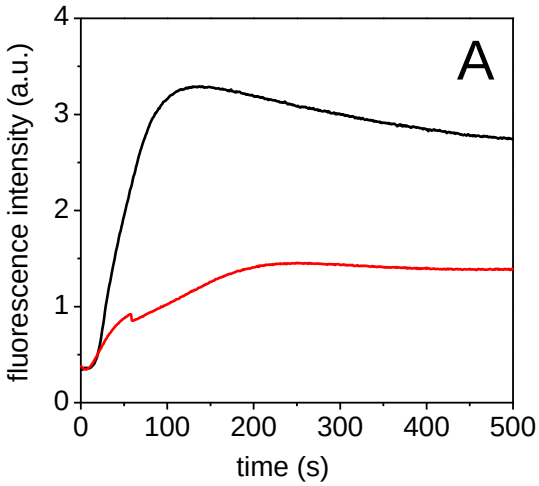

B

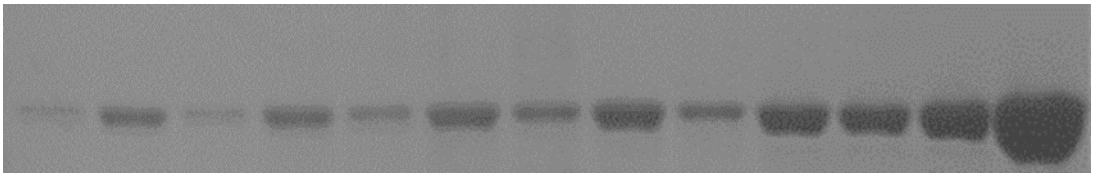

	1	2	3	4	5	6	7	8	9	10	11	12	13
Conditions	NP	P	NP	P	NP	P	NP	P	NP	P	NP	P	P
[MreB] (μM)	1.25	1.25	1.67	1.67	2.5	2.5	3.13	3.13	4.17	4.17	6.25	6.25	25

Figure 9.